SANDIA REPORT

SAND2000—8583
Unlimited Release
Printed October 2000

A Novel Three-Dimensional Contact Finite Element Based on Smooth Pressure Interpolations

Reese E. Jones and Panayiotis Papadopoulos

Prepared by
Sandia National Laboratories
Albuquerque, New Mexico 87185 and Livermore, California 94550

Sandia is a multiprogram laboratory operated by Sandia Corporation, a Lockheed Martin Company, for the United States Department of Energy under Contract DE-AC04-94AL85000.

Sandia National Laboratories

Issued by Sandia National Laboratories, operated for the United States Department of Energy by Sandia Corporation.

Available to DOE and DOE contractors from
Office of Scientific and Technical Information
P.O. Box 62
Oak Ridge, TN 37831

Prices available from (703) 605-6000
Web site: http://www.ntis.gov/ordering.htm

Available to the public from
National Technical Information Service
U.S. Department of Commerce
5285 Port Royal Rd
Springfield, VA 22161

NTIS price codes
Printed copy: A04
Microfiche copy: A01

SAND2000 - 8583
Unlimited Release
Printed October 2000

A Novel Three-Dimensional Contact Finite Element Based on Smooth Pressure Interpolations *

Reese E. Jones
Science-Based Materials Modeling Department
Sandia National Laboratories
P. O. Box 969
Livermore, CA 94551-0969

Panayiotis Papadopoulos
Department of Mechanical Engineering
University of California, Berkeley
Berkeley, CA 94720-1740

Abstract

This article proposes a new three-dimensional contact finite element which employs continuous and weakly coupled pressure interpolations on each of the interacting boundaries. The resulting formulation circumvents the geometric bias of one-pass methods, as well as the surface locking of traditional two-pass node-on-surface methods. A Lagrange multiplier implementation of the proposed element is validated for frictionless quasi-static contact by a series of numerical simulations.

Keywords: finite element method, three-dimensional contact, Lagrange multipliers.

---

* Accepted for publication in International Journal for Numerical Methods in Engineering on July 20, 2000.

This page intentionally left blank.

DISCLAIMER

Portions of this document may be illegible in electronic image products. Images are produced from the best available original document.

Contents

This page intentionally left blank.

1 Introduction

Most commercial finite element program employ node-on-surface algorithms for simulating contact between two deformable solids. Here, the impenetrability constraint is enforced by applying discrete forces at the nodes on one of the contacting surfaces (the "slave" surface) and equal-and-opposite reactions on the other (the "master" surface). One-pass versions of this strategy use only forces associated with the nodes of one designated slave surface, while two-pass versions apply the process twice (i.e., for both master/slave combinations) and superpose all resulting forces. It is known that such node-on-surface algorithms have certain intrinsic shortcomings. Clearly, one-pass algorithms are geometrically biased by the choice of a specific slave surface. On the other hand, two-pass algorithms generally over-constrain the contacting boundary surfaces, as noted by Kikuchi and Oden [1, p. 165]. This pathology will be referred to here as "surface locking". Moreover, in traditional node-on-surface algorithms the contact traction fields (e.g., pressure) are not directly approximated. Rather, they are typically recovered from the nodal forces as an afterthought by means of tributary area methods. This lack of smooth traction interpolations further inhibits any attempt towards a formal convergence analysis.

These shortcomings have motivated several alternative contact element formulations, see, e.g., [2, 3, 4, 5, 6], which employ piecewise continuous polynomial traction interpolations on the contact boundaries. These developments rely, to an extent, on element formulations developed and mathematically analyzed for a deformable body contacting a rigid surface (i.e. the Signorini problem) [7, 8, 9]. However, in sharp contrast to the Signorini problem, the use of smooth traction interpolations in two-body contact introduces additional complications stemming from the need to define these fields and numerically integrate their contributions on (usually irregular) segments of the element boundaries or on an arbitrarily chosen intermediate surface.

This article describes a novel finite element method for three-dimensional frictionless contact, which addresses the fundamental deficiencies of node-on-surface algorithms, while remaining amenable to robust computational implementation in a finite deformation setting. The proposed method departs from other continuous interpolation methods in two major ways: first, traction fields are chosen separately (although not independently) on each of the two contacting surfaces, so that traction continuity is enforced in a weak sense and integration schemes naturally arising from

the underlying domain elements can be readily employed. Second, the new contact element permits the exact transmission of constant pressure, thus unconditionally passing the contact patch test postulated in [10]. These element properties have been originally conceived and exploited in earlier work on two-dimensional contact [11, 12]. The resulting formulation is simple and efficient to implement in three-dimensions, as it requires only routine and inexpensive geometric computations. In addition, extensive numerical experimentation to date suggests that it yields stable results and effectively bypasses all problems related to surface locking.

The organization of the article is as follows: first, fundamentals of contact mechanics including a weak form of the governing equations are presented briefly as background. Then, the proposed contact element is introduced in connection with the standard eight-node hexahedral domain element. The fidelity of the algorithm is subsequently tested in a number of representative simulations, whose results are compared to analytical estimates, as well as to numerical results from certain one- and two-pass algorithms.

2 Elements of Contact Mechanics

Consider two deformable bodies $\mathcal{B}^\alpha$, $\alpha = 1, 2$, and let any material point $X^\alpha \in \mathcal{B}^\alpha$ be associated with position vector $\mathbf{X}^\alpha$ in a fixed reference configuration Ω_0^α. The region Ω_0^α in the Euclidean point space is simply connected and open with respect to the ambient metric, and its boundary is denoted by $\partial\Omega_0^\alpha$.

A smooth motion $\boldsymbol{\chi}^\alpha$ is defined for each body, such that $\mathbf{x}^\alpha = \boldsymbol{\chi}^\alpha(\mathbf{X}^\alpha, t)$, where $\mathbf{X}^\alpha \in \Omega_0^\alpha$ is mapped at time t to its image $\mathbf{x}^\alpha$ in the current configuration $\Omega^\alpha(t)$. The motion is taken to be invertible at fixed t, which implies that the deformation gradient $\mathbf{F}^\alpha = \frac{\partial \boldsymbol{\chi}^\alpha}{\partial \mathbf{X}^\alpha}$ is non-singular. In addition, $\boldsymbol{\chi}^\alpha$ maps the referential boundary region $\partial\Omega_0^\alpha$ onto its image $\partial\Omega^\alpha(t)$, which is assumed to be Lipschitz with outward unit normal $\mathbf{n}^\alpha$. For convenience, each point of $\partial\Omega^\alpha$ is associated with convected Gaussian coordinates $\xi_\gamma^\alpha, \gamma = 1, 2$.

Admitting quasi-static conditions, the equilibrium equations take the form

$$\operatorname{div} \mathbf{T}^\alpha + \rho^\alpha \mathbf{b}^\alpha \;=\; \mathbf{0} \quad \text{in } \Omega^\alpha \;, \tag{1}$$

where $\mathbf{T}^\alpha$ represents the Cauchy stress tensor, ρ^α the mass density in the current configuration, and $\mathbf{b}^\alpha$ the body force per unit mass. The motions of the two bodies

are also subject to the principle of impenetrability of matter [13], which stipulates that

$$\Omega^{(1)} \cap \Omega^{(2)} = \varnothing \,. \tag{2}$$

Consequently, the common boundary region $C(t) = \partial\Omega^{(1)} \cap \partial\Omega^{(2)}$ defines the contact interface. The remainder of the boundary $\partial\Omega^\alpha$ is composed of regions Γ_u^α and Γ_t^α, such that

$$\begin{aligned} \mathbf{u}^\alpha &= \bar{\mathbf{u}}^\alpha \quad \text{on } \Gamma_u^\alpha \,, \\ \mathbf{t}^\alpha &= \bar{\mathbf{t}}^\alpha \quad \text{on } \Gamma_t^\alpha \,, \end{aligned} \tag{3}$$

where $\mathbf{u}^\alpha = \mathbf{x}^\alpha - \mathbf{X}^\alpha$ is the displacement vector and $\mathbf{t}^\alpha_{\mathbf{n}^\alpha}$ the traction vector on the surface with outward unit normal $\mathbf{n}^\alpha$. This vector is related to the Cauchy stress tensor $\mathbf{T}^\alpha$ by $\mathbf{t}^\alpha_{\mathbf{n}^\alpha} = \mathbf{T}^\alpha \mathbf{n}^\alpha$.

The impenetrability condition (2) can be recast as a unilateral constraint by introducing a distance (or "gap") function g^α on the boundary of each body. To this end, define the point sets

$$\begin{aligned} \mathcal{V}_+^\alpha(\mathbf{x}^\alpha; \mathbf{n}^\alpha) &= \left\{ \mathbf{x}^\beta \in \partial\Omega^\beta \;\middle|\; (\mathbf{x}^\beta - \mathbf{x}^\alpha) \times \mathbf{n}^\alpha = \mathbf{0} \,,\; (\mathbf{x}^\beta - \mathbf{x}^\alpha) \cdot \mathbf{n}^\alpha \geq 0 \right\} , \\ \mathcal{V}_-^\alpha(\mathbf{x}^\alpha; \mathbf{n}^\alpha) &= \left\{ \mathbf{x}^\beta \in \partial\Omega^\beta \;\middle|\; (\mathbf{x}^\beta - \mathbf{x}^\alpha) \times \mathbf{n}^\alpha = \mathbf{0} \,,\; (\mathbf{x}^\beta - \mathbf{x}^\alpha) \cdot \mathbf{n}^\alpha < 0 \right\} , \end{aligned}$$

corresponding to the projections of $\mathbf{x}^\alpha$ on $\partial\Omega^\beta$ along the two rays defined by $\mathbf{n}^\alpha$. Here, $\beta = \text{mod}\,(\alpha, 2) + 1$ denotes the index of the opposing body*. Then, let $\check{\mathbf{x}}_+^\beta$ and $\check{\mathbf{x}}_-^\beta$ be the closest such projections, namely

$$\begin{aligned} \|\check{\mathbf{x}}_+^\beta - \mathbf{x}^\alpha\| &= \min_{\mathbf{x}^\beta \in \mathcal{V}_+^\alpha} \|\mathbf{x}^\beta - \mathbf{x}^\alpha\| \,, \\ \|\check{\mathbf{x}}_-^\beta - \mathbf{x}^\alpha\| &= \min_{\mathbf{x}^\beta \in \mathcal{V}_-^\alpha} \|\mathbf{x}^\beta - \mathbf{x}^\alpha\| \,. \end{aligned}$$

A single-valued distance function is specified as

$$g^\alpha = \begin{cases} (\check{\mathbf{x}}^\beta - \mathbf{x}^\alpha) \cdot \mathbf{n}^\alpha & \text{if } \mathcal{V}_+^\alpha \neq \emptyset \\ +\infty & \text{if } \mathcal{V}_+^\alpha = \emptyset \end{cases} , \tag{4}$$

*By expanding the set of potential contact points from $\partial\Omega^\beta$ to $\bigcup_{\iota=1}^{N} \partial\Omega^\iota \setminus \{\mathbf{x}^\alpha\}$, this definition can be trivially extended to self- and N-body contact.

where a unique projection $\check{\mathbf{x}}^\beta$ is defined as

$$\check{\mathbf{x}}^\beta \;=\; \begin{cases} \check{\mathbf{x}}^\beta_+ & \text{if } \check{\mathbf{n}}^\beta_+ \cdot \mathbf{n}^\alpha \leq 0 \\ \check{\mathbf{x}}^\beta_- & \text{if } \check{\mathbf{n}}^\beta_+ \cdot \mathbf{n}^\alpha > 0 \end{cases} , \tag{5}$$

see Figure 1. It follows from (4) and (5) that g^α vanishes identically on C. Also, the impenetrability constraint (2) takes the form

$$g^\alpha \;\geq\; 0 \quad \text{on } \partial\Omega^\alpha \, . \tag{6}$$

Clearly, letting

$$C^\alpha \;= \{\mathbf{x}^\alpha \in \partial\Omega^\alpha \quad | \quad g^\alpha = 0\} \, ,$$

it follows that $C^{(1)} = C^{(2)} = C$.

A separate equilibrium statement applies on the contact interface (see, e.g., [14]), in the form

$$[\![\mathbf{t}]\!]^\alpha_{\mathbf{n}^\alpha} \;=\; \check{\mathbf{t}}^\beta_{\mathbf{n}^\alpha} - \mathbf{t}^\alpha_{\mathbf{n}^\alpha} \;=\; \mathbf{0} \, , \tag{7}$$

where $\check{\mathbf{t}}^\beta_{\mathbf{n}^\alpha}$ denotes $\mathbf{t}^\beta_{\mathbf{n}^\alpha}(\check{\mathbf{x}}^\beta, t)$. For frictionless contact, the surface traction becomes

$$\mathbf{t}^\alpha_{\mathbf{n}^\alpha} \;=\; -p^\alpha \mathbf{n}^\alpha \, ,$$

where $p^\alpha \geq 0$ is the pressure[†]. Consequently, equation (7) reduces to

$$[\![p]\!]^\alpha \;=\; \check{p}^\beta - p^\alpha \;=\; 0 \, . \tag{8}$$

Furthermore, given

$$\dot{g}^\alpha \;=\; \left.\frac{\partial g^\alpha}{\partial t}\right|_{\xi^\alpha_\gamma} \;=\; [\![\mathbf{v}]\!]^\alpha \cdot \mathbf{n}^\alpha \, ,$$

where $[\![\mathbf{v}]\!]^\alpha = \check{\mathbf{v}}^\beta - \mathbf{v}^\alpha$ is the jump in velocity across C, it is clear that the rate of work done by the tractions on the contact surface C^α is

$$\mathbf{t}^\alpha \cdot [\![\mathbf{v}]\!]^\alpha \;=\; p^\alpha \dot{g}^\alpha \;=\; 0 \, .$$

Thus, the pressure p^α is work-conjugate to g^α and is identified as the Lagrange multiplier that enforces the (workless) impenetrability constraint $g^\alpha = 0$.

[†]Commonly, the contact pressure is denoted by the single field p, namely equilibrium on the singular surface C is assumed to hold at the outset. However, this direct reduction is not employed here for reasons that will become apparent as the finite element approximation is introduced in Section 4.

3 Weak Formulation

The governing equations (1) and (8), the boundary condition $(3)_2$ and the constraint (6) can be put in a weak (weighted-residual) form, such that the solution $(\mathbf{u}^\alpha, p^\alpha) \in U^\alpha \times P^\alpha$ satisfies

$$\sum_{\alpha=1,2} \Big\{ \int_{\Omega^\alpha} \left(\operatorname{grad} \mathbf{w}^\alpha \cdot \mathbf{T}^\alpha - \mathbf{w}^\alpha \cdot \rho^\alpha \mathbf{b}^\alpha\right) dv - \int_{\Gamma_q^\alpha} \mathbf{w}^\alpha \cdot \bar{\mathbf{t}}^\alpha \, da - \int_{\Gamma_c^\alpha} \mathbf{w}^\alpha \cdot (-p^\alpha \mathbf{n}^\alpha) \, da \Big\} = 0 , \quad (9)$$

$$\sum_{\alpha=1,2} \int_{\Gamma_c^\alpha} (q^\alpha - p^\alpha) g^\alpha \, da \geq 0 , \quad (10)$$

and

$$\int_C r \, [\![p]\!] \, da = 0 , \quad (11)$$

for all $(\mathbf{w}^\alpha, q^\alpha, r) \in W^\alpha \times Q^\alpha \times R$. Note that in equations (9)–(10) all integrals related to contact are written over the region $\Gamma_c^\alpha (\supset C^\alpha)$, which is defined as the union of those boundary regions on which no normal displacement or (inhomogeneous) traction boundary conditions are specified externally. The spaces of admissible displacements and associated weighting functions are chosen to be

$$\begin{aligned} U^\alpha &= \left\{ \mathbf{u}^\alpha \in H^1(\Omega^\alpha) \quad | \quad \mathbf{u}^\alpha = \bar{\mathbf{u}}^\alpha \ \text{ on } \Gamma_u^\alpha \right\} , \\ W^\alpha &= \left\{ \mathbf{w}^\alpha \in H^1(\Omega^\alpha) \quad | \quad \mathbf{w}^\alpha = \mathbf{0} \ \text{ on } \Gamma_u^\alpha \right\} , \end{aligned}$$

hence appealing to a standard trace theorem (see, e.g., [15]), the traces $\mathbf{u}^\alpha \cdot \mathbf{n}^\alpha$ and $\mathbf{w}^\alpha \cdot \mathbf{n}^\alpha$ used in (4) and (9) can be viewed as continuous linear operators from $H^1(\Omega^\alpha)$ to $H^{1/2}(\partial\Omega^\alpha)$. The spaces of admissible pressures and weights are now defined as

$$\begin{aligned} P^\alpha &= \left\{ p^\alpha \in H^{-\frac{1}{2}}(\Gamma_c^\alpha) \quad | \quad p^\alpha \geq 0 \, , \ p^\alpha = 0 \ \text{ on } \Gamma_c^\alpha \setminus C^\alpha \right\} , \\ Q^\alpha &= \left\{ q^\alpha \in H^{-\frac{1}{2}}(\Gamma_c^\alpha) \quad | \quad q^\alpha \geq 0 \right\} , \\ R &= \left\{ r \in H^{\frac{1}{2}}(C) \right\} . \end{aligned}$$

Note that equations (9) and (10), when restricted to a single deformable body (i.e., $\alpha = 1$ or 2), are identical in structure to those arising from the Signorini problem. The two Signorini-like problems in (9) and (10) are coupled by the definition of g^α and by equation (11).

4 A New Contact Element

The finite element formulation described in this section relies critically on the use of the weak formulation in equations (9)–(11) in conjunction with separate continuous pressure interpolations on each surface. In this case, it will be shown that the boundary integrals on Γ_c^α in (9) can be conveniently evaluated for each body using only the discretization naturally derived from its domain.

4.1 Discrete fields and equations of motion

The discrete counterparts of U^α and W^α defined in Section 3 are generally taken to be

$$\begin{aligned} U_h^\alpha &= \left\{ \mathbf{u}_h^\alpha \in H^1(\Omega_h^\alpha) \cap C^0(\Omega_h^\alpha) \quad | \quad \mathbf{u}_h^\alpha(\Omega_e^\alpha) \in \mathcal{P}_k(\Omega_e^\alpha) \ , \ \mathbf{u}_h^\alpha = \bar{\mathbf{u}}_h^\alpha \ \text{ on } \Gamma_{u,h}^\alpha \right\} , \\ W_h^\alpha &= \left\{ \mathbf{w}_h^\alpha \in H^1(\Omega_h^\alpha) \cap C^0(\Omega_h^\alpha) \quad | \quad \mathbf{w}_h^\alpha(\Omega_e^\alpha) \in \mathcal{P}_k(\Omega_e^\alpha) \ , \ \mathbf{w}_h^\alpha = \mathbf{0} \ \text{ on } \Gamma_{u,h}^\alpha \right\} , \end{aligned}$$

where $\mathcal{P}_k$ denotes the space of polynomials complete to degree k and Ω_e^α the domain of element e. Similarly,

$$\begin{aligned} P_h^\alpha &= \left\{ p_h^\alpha \in H^{-\frac{1}{2}}(\Gamma_{c,h}^\alpha) \cap C^0(\Gamma_{c,h}^\alpha) \quad | \quad p_h^\alpha(\partial\Omega_e^\alpha) \in \mathcal{P}_k(\partial\Omega_e^\alpha) \ , \right. \\ &\qquad \left. p_h^\alpha \geq 0 \ , \ \ p_h^\alpha = 0 \ \text{ on } \Gamma_{c,h}^\alpha \setminus C_h^\alpha \right\} , \\ Q_h^\alpha &= \left\{ q_h^\alpha \in H^{-\frac{1}{2}}(\Gamma_{c,h}^\alpha) \cap D(\Gamma_{c,h}^\alpha) \quad | \quad q_h^\alpha \geq 0 \right\} , \\ R_h &= \left\{ r_h \in (P_h^\alpha)^\star \cap D(C_h) \right\} , \end{aligned}$$

where $\mathcal{P}_k(\partial\Omega_e^\alpha)$ denotes the space of polynomials on $\partial\Omega_e^\alpha$ complete to degree k, $(P_h^\alpha)^\star$ the dual of P_h^α, and $D(\Gamma_{c,h}^\alpha)$ (resp. $D(C_h)$) the space of Dirac distributions on $\Gamma_{c,h}^\alpha$ (resp. C_h)[‡]. The choice of admissible displacements is routine for C^0-continuous domain finite elements. On the other hand, the assumed C^0-continuity of the pressures departs in a fundamental way from classical node-on-surface treatments, see the Appendix. In addition, the choice of R_h implies weak, collocation-based satisfaction of the equilibrium equation on C_h.

Employing the notation $\underline{\mathbf{u}}^\alpha$ and $\underline{p}^\alpha$ for global vectors of nodal quantities, standard finite element interpolations can be introduced for the displacement field and its

[‡]Note that for the given choices of discrete admissible functions, the duality pairing in (11) is well-defined despite the fact that $R_h \not\subset R$.

gradient as

$$\begin{aligned} \mathbf{u}_h^\alpha(\mathbf{x},t) &= \mathbf{N}^\alpha(\mathbf{x})\,\underline{\mathbf{u}}^\alpha(t)\ , \\ \operatorname{grad}\mathbf{u}_h^\alpha(\mathbf{x},t) &= \mathbf{B}^\alpha(\mathbf{x})\,\underline{\mathbf{u}}^\alpha(t)\ , \end{aligned} \tag{12}$$

as well as for the (continuous) contact pressure as

$$p_h^\alpha(\xi_\gamma^\alpha,t) = \mathbf{L}^\alpha(\xi_\gamma^\alpha)\,\underline{p}^\alpha(t)\ . \tag{13}$$

Analogous interpolations apply to the respective weighting functions $\mathbf{w}_h^\alpha$ and the gap functions, leading to global vectors $\underline{\mathbf{w}}^\alpha$ and $\underline{g}^\alpha$, respectively. To ensure consistency with the continuous pressures in (13), the interpolated gap fields g_h^α are made single-valued everywhere on Γ_c^α by employing arithmetically averaged outward normals $\mathbf{n}^\alpha$ at all inter-element boundaries.

The discrete counterparts of the weighting functions q^α and r must be chosen to avoid over-constraining the boundary surfaces $\partial\Omega_h^\alpha$. These piecewise smooth surfaces are in general non-conforming, see Figure 2 for an illustration. Exceptions may occur in the certain special cases of "node-on-node" contact, as well as when the contact surface takes on a low-order *global* polynomial form that is exactly representable by the surface discretizations of both bodies. However, in the general case where the boundary nodes are not aligned and the contact surface takes an arbitrary shape, *surface locking* occurs when the impenetrability constraint is enforced at every nodal point on C_h. This pathology is analogous to the over-constraining of the discrete displacement field in incompressible elasticity, a problem that has been studied extensively by the finite element community. To date, formal convergence analysis of two-body contact has received relatively little attention, owing to the adherence to force-based node-on-surface methods as well as to the complexity of dealing with the interaction of two arbitrarily chosen meshes.

In practice, global surface-locking may be prevented by enforcing the impenetrability constraint selectively on C_h^α. This is accomplished by effecting a regular partition of nodes on C_h^α into two disjoint sets $\mathcal{S}_g^\alpha$ and $\mathcal{S}_p^\alpha$. The discrete counterparts of the weighting functions q^α and r in (10) and (11) are approximated according to

$$q_h^\alpha(\mathbf{x},t) = \sum_{I\in\mathcal{S}_g^\alpha} \delta(\mathbf{x}_I^\alpha) q_I^\alpha(t) = \mathbf{Q}^\alpha(\mathbf{x})\,\underline{q}(t)\ , \tag{14}$$

$$r_h(\mathbf{x},t) = \sum_{\alpha=1,2}\sum_{I\in\mathcal{S}_p^\alpha} \delta(\mathbf{x}_I^\alpha) r_I^\alpha(t) = \mathbf{R}(\mathbf{x})\,\underline{r}(t)\ , \tag{15}$$

where $\mathbf{Q}^\alpha$ and $\mathbf{R}$ are row vectors of Dirac-delta functions and $\mathbf{x}_I^\alpha$ denotes the position of node I on surface C_h^α.

Taking into account the interpolations in (12)–(15), the weighted-residual equations (9)-(11) give rise to the discrete equations

$$\mathrm{f}_u = \sum_{\alpha=1,2} \Big\{ \int_{\Omega_h^\alpha} (\mathbf{B}^{\alpha T}\mathbf{T}^\alpha - \mathbf{N}^{\alpha T}\rho^\alpha \mathbf{b})\, dv - \int_{\Gamma_{q,h}^\alpha} \mathbf{N}^{\alpha T}\bar{\mathbf{t}}^\alpha\, da - \int_{C_h^\alpha} \mathbf{N}^{\alpha T}(-p_h^\alpha \mathbf{n}^\alpha)\, da \Big\} = \mathbf{0}\,, \quad (16)$$

$$\mathrm{f}_g = \sum_{\alpha=1,2} \int_{C_h^\alpha} \mathbf{Q}^{\alpha T} g^\alpha\, da = \mathbf{0}\,, \quad (17)$$

and

$$\mathrm{f}_p = \int_{C_h} \mathbf{R}^T [\![p_h]\!]\, da = \mathbf{0}\,. \quad (18)$$

The component forms of equations (17) and (18) are

$$g^\alpha(\mathbf{x}_I^\alpha) = 0 \quad \text{for every } I \in \mathcal{S}_g^\alpha,\ \alpha \in 1,2\,, \quad (19)$$

$$[\![p_h]\!](\mathbf{x}_I^\alpha) = 0 \quad \text{for every } I \in \mathcal{S}_p^\alpha,\ \alpha \in 1,2\,, \quad (20)$$

respectively. Clearly, $\mathcal{S}_g^\alpha$ (resp. $\mathcal{S}_p^\alpha$) consists of all boundary nodes on which the impenetrability constraint (resp. the pressure continuity condition) is enforced.

4.2 Application to eight-node hexahedral elements

In the remainder of this article, attention is focused on four-node bilinear quadrilateral contact elements arising naturally from a domain approximation using standard eight-node hexahedral domain elements. There are at least two boundary node partitioning techniques for two-dimensional surfaces that can be readily employed in connection with the enforcement of (10) and (11). The first involves the construction of a continuous curve that traces the topology of C_h^α and passes through each node only once. This is a Peano-Hilbert space-filling curve [16], and provides a simple means of assigning nodes to the sets $\mathcal{S}_g^\alpha$ and $\mathcal{S}_p^\alpha$. For instance, nodes with odd ordinal may belong to $\mathcal{S}_g^\alpha$, while nodes with even ordinal may belong to $\mathcal{S}_p^\alpha$, as seen in Figure 3. Alternatively, the surface mesh can be "tiled" in a recursive manner using the reference

element shown in Figure 4 to produce the nodal partition. Each method requires a "seed" node or element to start the patterning, thus does not produce a unique pattern on a given mesh. However, for sufficiently regular meshes and corresponding seeds, the two methods yield identical patterns. Clearly, the quality of a solution depends crucially on attaining a uniform spatial distribution of nodes with gap and pressure collocations. This guarantees a balanced enforcement of the impenetrability constraint and the continuity of normal traction. In addition to circumventing surface locking, such a balance is essential in order to ensure that the computed tractions do not bias the solution towards either of these two requirements. Both partitioning techniques provide such even distributions, where exactly two nodal pressure variables enforce gap constraints on every four-node surface element. Other patterns are possible where the nodal pressure variables associated with gap constraints and the nodal pressure variables satisfying pressure continuity across the contact surface are not equally divided.

With reference to Figure 4, the interpolation of p_h^α on the given element boundary is chosen to be

$$p_h^\alpha \;=\; \begin{cases} \displaystyle\sum_{i=1,2,3} L_i^{<123>}(\xi_\gamma^\alpha)\, p_i^\alpha & \text{if } \xi_1^\alpha \geq \xi_2^\alpha \\ \displaystyle\sum_{i=1,3,4} L_i^{<134>}(\xi_\gamma^\alpha)\, p_i^\alpha & \text{if } \xi_1^\alpha < \xi_2^\alpha \end{cases} ,$$

where $L_i^{<123>}$ and $L_i^{<134>}$ are the linear interpolation functions for triangles (1-2-3) and (1-3-4), respectively. The support of the interpolation function associated with any node in $\mathcal{S}_p^\alpha$, e.g., node 4 in Figure 5, is local to elements associated with the node and is bounded by nodes in $\mathcal{S}_g^\alpha$. Within the support region of such a "traction continuity" node, the collocation equation

$$p_h^\alpha(\check{\xi}_\gamma^\alpha) \;=\; p_h^\beta \,,$$

derived from (18), can be explicitly solved for the undetermined pressure. Indeed, with reference to Figure 5, let "I" be the projection on $\Gamma_{c,h}^\alpha$ of the node I in $\mathcal{S}_p^\beta$ which lies closest to node 4 of $\mathcal{S}_p^\alpha$ and inside its support region[§]. Then,

$$p_4^\alpha \;=\; \frac{1}{L_4^{<134>}}(p_I^\beta - L_1^{<134>} p_1^\alpha - L_3^{<134>} p_3^\alpha) \,,$$

[§]In this work, all projections and gap calculations use the exact geometry of the boundary surfaces of the hexahedral elements.

where p_I^β is the pressure at node I. If no such closest projection exists, a linear interpolation of p^α is made within the support region of the "pressure continuity" node.

In order for the pressure approximation of a contact finite element to satisfy polynomial completeness requirements, it is necessary that the element pass the patch test proposed in [10]. This necessitates that the formulation be able to transmit, independently of the discretization, a uniform pressure $-p_0^\alpha \mathbf{n}_0^\alpha$ through a flat contact surface C_h. An examination of the contact integral in (16), namely

$$-\int_{C_h^\alpha} \mathbf{N}^{\alpha T}(-p_h^\alpha \mathbf{n}^\alpha)\, da \;=\; p_0^\alpha \int_{C_h^\alpha} \mathbf{N}^{\alpha T}(\xi_\gamma^\alpha)\, j(\xi_\gamma^\alpha)\, d\xi_1^\alpha d\xi_2^\alpha \;\mathbf{n}_0^\alpha \;,$$

reveals that satisfaction of the patch test requires exact integration of a quantity of order $O(\xi_1^2\xi_2, \xi_1\xi_2^2)$ over the intersection $C^\alpha \cap \partial\Omega_e^\alpha$, where the element boundaries are used as integration cells. In case an element boundary is in full contact, this condition can be satisfied by several integration schemes[¶].

The case of element boundaries in partial contact, i.e. $C^\alpha \cap \partial\Omega_e^\alpha \subset \partial\Omega_e^\alpha$, is more complex, given the potentially irregular geometry of the contact boundary. A "quasi-element" that relies on a triangularization of the contact region and linear approximation between known pressure samplings, e.g. nodes 2,3 and node K from the opposing surface in Figure 6, has been developed to handle partial contact. This treatment allows finite jumps in pressure at the boundary of the contact region C_h, which is necessary where the boundary of a contacting body is non-smooth at the edge of contact, as is the case in punch problems[‖]. Moreover, this quasi-element treatment allows exact and unqualified satisfaction of the patch test. It should be noted that, given the computational expense of triangularization, there may be a practical limit to how accurately one needs to resolve a highly irregular contact boundary within a single quasi-element. Indeed, the error induced in the contact residual by ignoring the contributions of elements that are partially in contact is of order h^2, where h is the mesh size parameter.

[¶]A 2 x 2 Gaussian scheme as well as a nodal quadrature scheme derived from the shape functions of a two-dimensional eight-node serendipity element have been employed successfully.

[‖]A similar treatment can be employed in the interior of C in the case of material discontinuities within the contacting bodies.

5 Numerical Simulations

To demonstrate the performance of the proposed contact element, a sequence of simulations have been conducted using FEAP [17]. First, the contact patch test is used to verify the algorithm's consistency with the continuum problem. Subsequently, problems involving non-homogeneous deformation and non-flat contact interfaces are used for independent validation of the formulation.

In each simulation, linear eight-node isoparametric hexahedral elements are used to discretize the contacting bodies. These elements are endowed with a compressible, isotropic neo-Hookean hyperelastic constitution suitable for finite deformation. The strain energy for this material takes the form

$$W \;=\; \frac{1}{2}\lambda(\det^{\frac{1}{2}}\mathbf{C}-1)^2+\frac{1}{2}\mu(\mathrm{tr}\,\mathbf{C}-3)-\mu\ln(\det^{\frac{1}{2}}\mathbf{C})\;,$$

where $\mathbf{C}=\mathbf{F}^T\mathbf{F}$ is the right Cauchy-Green deformation tensor. Also, λ,μ are material constants which correspond to the Lamé constants at infinitesimal deformations and are related to Young's modulus E and Poisson's ratio ν by $\lambda=\frac{E\nu}{(1+\nu)(1-2\nu)}$ and $\mu=\frac{E}{2(1+\nu)}$.

The discrete governing equations are solved using a full Newton-Raphson iteration scheme. At each iteration, the surface momentum balance equation (18) is satisfied by collocation. The remaining non-linear algebraic equations (16) and (17) are linearized about the current state $[\underline{\mathbf{u}},\underline{p}]^T_{(i)}$, i.e.,

$$\left[\begin{array}{cc} D_u\mathbf{f}_u & D_p\mathbf{f}_u \\ \theta D_u\mathbf{f}_g & \mathbf{0} \end{array}\right]_{(i)}\left[\begin{array}{c} \triangle\underline{\mathbf{u}} \\ \triangle\underline{p} \end{array}\right]_{(i)} \;=\; -\left[\begin{array}{c} \mathbf{f}_u \\ \theta\mathbf{f}_g \end{array}\right]_{(i)}\;, \tag{21}$$

where the parameter $\theta>0$ is employed to improve the conditioning of the overall system. In the special case of "node-on-node" contact, equation (21) leads to a symmetric system; however, in general, the system (21) is unsymmetric due to the misalignment of the discretizations on the interacting bodies. Since the nodal partitioning (19) is merely a pre-processing step, the cost of storing and solving these unsymmetric linear systems presents the only significant additional expense of the proposed approach relative to other Lagrange multiplier formulations for frictionless contact.

As noted in [12], the submatrix $D_u\mathbf{f}_u$ in (21) may be singular, see, e.g., the contact patch test of Section 5.2. This prevents the direct solution of (21) without pivoting.

This problem can be remedied by writing the equations equivalently as

$$\left[\begin{array}{cc} D_u\mathbf{f}_u + \omega(D_u\mathbf{f}_g)^T D_u\mathbf{f}_g & D_p\mathbf{f}_u \\ \theta D_u\mathbf{f}_g & \mathbf{0} \end{array}\right]_{(i)} \left[\begin{array}{c} \triangle\underline{\mathbf{u}} \\ \triangle\underline{p} \end{array}\right]_{(i)} = -\left[\begin{array}{c} \mathbf{f}_u + \omega(D_u\mathbf{f}_g)^T\mathbf{f}_g \\ \theta\mathbf{f}_g \end{array}\right]_{(i)}, \quad (22)$$

where $\omega > 0$ is an additional conditioning parameter. The simultaneous solution of the linear system (22) for $[\triangle\underline{\mathbf{u}}, \triangle\underline{p}]^T_{(i)}$ is used to update the current state according to

$$\left[\begin{array}{c} \underline{\mathbf{u}} \\ \underline{p} \end{array}\right]_{(i+1)} = \left[\begin{array}{c} \underline{\mathbf{u}} \\ \underline{p} \end{array}\right]_{(i)} + \left[\begin{array}{c} \triangle\underline{\mathbf{u}} \\ \triangle\underline{p} \end{array}\right]_{(i)}.$$

Convergence of the iterative scheme is assessed by the Euclidean norm of the reduced residual vector $[\mathbf{f}_u + \omega(D_u\mathbf{f}_g)^T\mathbf{f}_g,\ \theta\mathbf{f}_g]^T_{(i)}$.

5.1 A Patch Test for Two-body Contact

As in reference [18], the patch test consists of two rectangular parallelepipeds in contact with uniform normal traction applied throughout their exposed upper surfaces. The Lamé constants $\lambda = 5.77 \times 10^2$ GPa and $\mu = 3.85 \times 10^2$ GPa for both bodies are chosen to correspond to Young's modulus $E = 1.0 \times 10^3$ GPa and Poisson's ratio $\nu = 0.3$. The objective of this test is to verify that the proposed formulation satisfies the completeness requirement in the sense of [10], namely that it allows the exact transmission of constant pressure.

The algorithm was tested using a variety of relative discretizations and orientations of the two bodies. In each case, the formulation effected a uniform normal traction on the flat contact interface to within machine precision. The resulting homogeneous deformation for a typical mesh is seen in Figure 7. Note that, in the given example, the surface elements on the lower body are in partial contact while the surface elements of the upper body are chosen to have non-constant Jacobians.

5.2 Rectangular Punch on Elastic Foundation

Let two rectangular parallelepipeds be placed in contact, as shown in Figure 8. The top body (punch) is brought into contact with the bottom body (foundation) via prescribed normal displacements on its upper surface. The punch has dimensions 5m × 5m × 1m and is meshed uniformly using 6 × 6 × 2 elements with two mutually

orthogonal vertical symmetry planes. Likewise, the foundation has dimensions 7m $\times$ 7m $\times$ 2m and a uniform mesh of $14 \times 14 \times 2$ elements. The stiffness ratio between the two bodies is $\kappa = \frac{E_{\text{punch}}}{E_{\text{found}}} = 10.0$, where $E_{\text{found}} = 1.0 \times 10^3$ GPa. Also, Poisson's ratio is fixed at $\nu = 0.3$.

The resulting pressure field is depicted in Figure 9 and clearly approximates the boundary singularity due to the indentation of the punch. Figure 9 further demonstrates that the weak satisfaction of the pressure continuity across the contact interface is remarkably accurate. The formulation also allows for a stable recovery of the limit of a rigid punch indenting a deformable foundation. Indeed, Figure 10 shows the pressure field on the foundation for the cases $\kappa = 10.0, 100.0, \infty$ ($\kappa = \infty$ corresponds to the punch being rigid). It is apparent that the solution for $\kappa = 100.0$ is already quite close to the rigid punch limit.

5.3 Hertzian Contact of Two Deformable Bodies

Two identical bodies are pressed together through prescribed displacements. The bodies are meshed identically with $12 \times 12 \times 2$ elements and their contacting surfaces are approximately spherical with radius of curvature 120m, as seen in Figure 11. Also, the elastic constants of both bodies are chosen to be $\lambda = 5.77 \times 10^4$ GPa and $\mu = 3.85 \times 10^4$ GPa. Note that the initial configurations of the bodies are rotated by 45° relative to each other in order to prevent fortuitous node alignment. Also, in order to accurately capture bending-like deformation modes, it was deemed necessary to add piece-wise quadratic incompatible modes to the interpolation functions of the domain elements, as in [19].

Figure 12 shows pressure fields at forced normal approach of 0.3m which are smooth and nearly identical on both surfaces**. These fields compare well both in terms of the region of contact and the pressure distribution with the classical Hertzian solution, as seen in Figure 13††.

A second analysis is performed to compare the proposed formulation with a one-

**The pressure fields are graphed relative to horizontal x-y axes parallel to the sides of the upper body.

††The negative pressures at the edge of contact on the upper surface are caused by extrapolation at a nodal pressure determined by collocation, which is not subject to $p \geq 0$. Such edge effects are inevitable for arbitrary node alignment and are reduced with mesh refinement.

pass counterpart employing the equivalent nodal force method of momentum transfer described in the Appendix. Here, the stiffness of the lower body is decreased by an order of magnitude and the radius of curvature of both bodies is decreased from 120m to 30m so that the contact surface is ensured to be substantially non-flat. Also, to investigate the performance under non-uniform relative mesh density, the resolution in the lower body is increased to $16 \times 16 \times 2$ elements and that of the upper body is decreased from to $10 \times 10 \times 2$ elements, see Figure 14. The deformed mesh using the proposed method is shown in Figure 15. It is seen from Figure 16 that the pressure profile generated by the proposed method compares well to one resulting from a one-pass Lagrange multiplier formulation that uses the more finely discretized lower surface as the surface of integration. However, it is also clear from Figure 17 that a one-pass formulation in which the upper (coarser) surface is designated as the surface of integration yields a significantly inferior solution. In particular, since gap constraints are only enforced at the nodes of the upper surface, there exist large penetrations of the lower surface's nodes along the contact surface which adversely affect the solution, see Figure 18. This geometric bias of one-pass algorithms is completely circumvented by the proposed approach.

5.4 Inflation of Concentric Rings in Contact

A system of two concentric rings which are in contact at no initial tractions is inflated by subjecting the inner ring to outward radial displacement. The rings have inner radii $R_i^i = 4.0$m and $R_i^o = 5.02$m, with common thicknesses $t = 1.0$m and depth $d = 10.0$m. A small initial separation between the rings is introduced to avoid penetration in the initial configuration. The material parameters $\lambda = 5.77 \times 10^2$ GPa and $\mu = 3.85 \times 10^2$ GPa are identical for both bodies. Using horizontal and vertical symmetry planes, the inner cylinder is meshed with 12 elements circumferentially, 2 elements in the depth and 1 element in the thickness. Likewise, the outer cylinder is meshed with 16 elements circumferentially, 3 elements in the depth and 1 element in the thickness.

Using the proposed method, both the deformation of the two cylinders and the pressure fields are uniform to within the smoothness and order of the the boundary discretization, see Figures 19 and 20 [‡‡]. On the other hand, if the two-pass penalty

[‡‡]Note that arclength is used to parameterize the circumferential direction in the `pressureplots`.

method described in the Appendix is employed with penalty $\epsilon = 1.0 \times 10^2$, a uniform pressure field can also be obtained, see Figure 21, albeit with an order of magnitude difference in the pressures compared to the Lagrange multiplier solution and accompanied by large violations of the impenetrability constraint. An increase of the penalty parameter to $\epsilon = 5.0 \times 10^2$ results in erratic and highly oscillatory pressure profiles suggestive of over-constrained surfaces, see Figure 22. A further increase in the penalty parameter of this two-pass simulation does not produce convergent solutions. This example illustrates the stability issue associated with two-pass approximations that are potentially hidden when a penalty regularization is used to enforce the impenetrability constraint. Again, the proposed reduced constraint method appears to be completely free of such a deficiency.

6 Conclusions

A systematic means has been devised for satisfying the impenetrability constraint and constructing a basis for the contact pressure fields in three-dimensional finite elements. The new approach alleviates the geometric bias and surface locking problems of many traditional methods. Furthermore, the simple scheme that employs boundary faces of the underlying domain elements for integration is shown to be sufficient to satisfy the contact patch test and provides a robust and efficient framework for accurate three-dimensional computations.

Acknowledgements

This work was funded by the Engineering Sciences Research Foundation at Sandia National Laboratories. This support is gratefully acknowledged. Sandia is a multiprogram laboratory operated by Sandia Corporation, a Lockheed Martin Company, for the United States Department of Energy under contract DE-ACO4-94AL85000.

Appendix: Node-on-surface Contact Treatments

Equilibrium on C implies continuity of the normal traction, see equation (8). In order to circumvent the need to explicitly introduce pressure interpolations, node-on-surface treatments attempt to apply this condition directly to the equivalent nodal forces of the two meshes along C_h. In this Appendix, traditional and non-traditional node-on-surface algorithms are examined in connection with the formulation of the governing equations developed in Section 3.

To derive node-on-surface formulations consistently with equations (9)-(11), let U_h^α, W_h^α P_h^α and Q_h^α be again defined as in Section 4. The key characteristic of a node-on-surface algorithm in the present context is the definition of the weighting function $r_h \in R_h$. Specifically, let

$$r_h \;=\; \sum_{\mathbf{x}_I^\alpha \in \Gamma_{c,h}^\alpha} \phi_I^\alpha r_I^\alpha \;=\; \mathbf{\Phi}^\alpha \underline{r}^\alpha \;, \tag{23}$$

where ϕ_I^α denotes the restriction on $\Gamma_{c,h}^\alpha$ of the standard domain interpolation function associated with boundary node I.

Taking into account the preceding choices of admissible fields, the equivalent nodal force $\mathbf{F}_I^\alpha$ at I due to contact is found from (9) to be

$$\mathbf{F}_I^\alpha \;=\; \int_{\Gamma_{c,h}^\alpha} \phi_I^\alpha (-p^\alpha \mathbf{n}^\alpha)\, da \;.$$

Employing nodal quadrature, $\mathbf{F}_I^\alpha$ can be approximated by

$$\mathbf{F}_I^\alpha \;\doteq\; (-p_I^\alpha \mathbf{n}_I^\alpha) \sum_e j_e^\alpha \, w_e^\alpha \;,$$

where p_I^α and $\mathbf{n}_I^\alpha$ denote the pressure and the outward unit normal at I, respectively. Also, in the previous equation $j_e^\alpha = \det [\frac{\partial \mathbf{x}_\gamma^\alpha(\xi_i^\alpha)}{\partial \xi_\delta^\alpha}]_e$ is the piecewise continuous surface Jacobian and w_e the integration weight for element e at node I. In addition, use of nodal quadrature on C^α in equation (10) directly implies that the constraint of impenetrability is enforced at all nodal points $\mathbf{x}_I^\alpha$. Finally, equation (11) becomes

$$\int_C \phi_I^\alpha [\![p]\!]\, da \;=\; 0 \;. \tag{24}$$

Ignoring the difference in direction between $\mathbf{n}^\alpha$ and $-\mathbf{n}^\beta$, equation (24) can be interpreted in terms of equivalent nodal forces as

$$\mathbf{F}_I^\alpha \;=\; -\int_{C^\alpha} \phi_I^\alpha p^\alpha \mathbf{n}^\alpha \, da \;=\; \int_{C^\beta} \phi_I^\alpha p^\beta \mathbf{n}^\beta \, da \;. \tag{25}$$

The right-hand side of equation (25) provides a precise rule for distributing $\mathbf{F}_I^\alpha$ on $\partial\Omega_h^\beta$. In particular, consistent equivalent nodal forces due to contact can be calculated on $\partial\Omega_h^\beta$ by first projecting ϕ_I^α on the interpolation functions ϕ_I^β associated with the nodes lying on $\partial\Omega_h^\beta$, then evaluating the resulting integrals. Except for very special cases, such equivalent nodal forces are <u>not</u> "equivalent" to those resulting from first applying $-\mathbf{F}_I^\alpha$ to the projection of node I on $\partial\Omega_h^\beta$ and then distributing $-\mathbf{F}_I^\alpha$ on $\partial\Omega^\beta$ by the rule

$$\mathbf{F}_J^\beta \;=\; \phi_J^\beta(-\mathbf{F}_I^\alpha)\;, \tag{26}$$

as is routinely done in traditional node-on-surface implementations. Therefore, this procedure leads to violation of the discrete counterpart of (11)*.

The preceding analysis pertains to one-pass node-on-surface formulations. Corresponding two-pass formulations can be obtained by integrating (10) using nodal quadrature over the boundary nodes of both surfaces and letting the weighting function r_h be defined as

$$r_h \;=\; \sum_{\alpha=1,2}\;\sum_{\mathbf{x}_I^\alpha\in\Gamma_{c,h}^\alpha} \phi_I^\alpha r_I^\alpha \;=\; \sum_{\alpha=1,2} \mathbf{\Phi}^\alpha \underline{r}^\alpha\;,$$

This, in effect, amounts to repeating the traction distribution twice, each time with one of the two surfaces providing the equivalent nodal forces and the other distributing them to its boundary nodes according to (25) or, incorrectly, (26).

A traction-based (as opposed to resultant force-based) one-pass algorithm, which is consistent with the discrete counterpart of equation (11), can be obtained as follows: first, with reference to (23), admit a pressure interpolation on Γ_c^α in the form

$$p^\alpha \;=\; \mathbf{\Phi}^\alpha \underline{p}^\alpha\;. \tag{27}$$

Then, the pressure p^α is determined at all nodal points of Γ_c^α by defining q_h^α with the aid of (14) as a sum of Dirac-delta functions taken precisely at these nodal points and, subsequently, enforcing the discrete counterpart of (10). On the other hand,

*The application of equal-and-opposite resultant forces is often justified by appealing to some form of Newton's third law, where the element nodes play the role of mass particles. Of course, no such law holds true in continuum mechanics. Rather, linear momentum balance can be invoked to <u>derive</u> the traction continuity condition (7).

nodal values of p^β are determined on Γ_c^β by collocation with p^α, corresponding to the choice

$$r_h = \sum_{\mathbf{x}_J^\beta \in \Gamma_{c,h}^\beta} r_J^\beta \delta(\mathbf{x}_J^\beta) \ .$$

A corresponding two-pass algorithm may be defined in an analogous fashion: the pressures p^α and p^β satisfy the nodal gaps g_I^α and g_J^β of both surfaces. However, in this case, a consistent construction using the interpolations (27) employed in the continuous one-pass algorithm is problematical. Indeed, if the pressures p^α and p^β are determined so $g_I^\alpha = 0$ and $g_J^\beta = 0$ at each node on C^α and C^β, then it is not, in general, possible to additionally satisfy the weak surface balance (11). In this case, the two simultaneous Signorini-like problems are very weakly coupled, with the only coupling between p^α and p^β being derived from the similarity of the gap functions g^α and g^β. To effect this gap-based coupling of the pressure fields in a direct fashion, a penalty formulation can be employed, such that

$$p^\alpha = \epsilon g^\alpha \ ,$$

where $\epsilon > 0$ is the penalty coefficient.

Numerical results using the above one- and two-pass algorithms are included in Section 5 to provide a basis for assessing the accuracy of the proposed formulation.

References

[1] N. Kikuchi and J.T. Oden. *Contact Problems in Elasticity : a Study of Variational Inequalities and Finite Element Methods.* SIAM, Philadelphia, 1988.

[2] J.C. Simo, P. Wriggers, and R.L. Taylor. A perturbed Lagrangian formulation for the finite element solution of contact problems. *Comp. Meth. Appl. Mech. Engrg.*, 50:163–180, 1985.

[3] P. Papadopoulos and R.L. Taylor. A mixed formulation for the finite element solution of contact problems. *Comp. Meth. Appl. Mech. Engrg.*, 94:373–389, 1992.

[4] G. Zavarise and P. Wriggers. A segment-to-segment contact strategy. *Math. Comp. Modeling*, 28:497–515, 1998.

[5] A.M. Habraken and S. Cescotto. Contact between deformable solids: The fully coupled approach. *Math. Comp. Modeling*, 28:153–169, 1998.

[6] F.B. Belgacem, P. Hild, and P. Laborde. Extension of the mortar finite element method to a variational inequality modeling unilateral contact. *Math. Models Meth. Appl. Sci.*, 9:287–303, 1999.

[7] Y.J. Song, J.T. Oden, and N. Kikuchi. Discrete LBB-conditions for RIP-finite element methods. TICOM Rep. 80-7, The University of Texas at Austin, 1980.

[8] N. Kikuchi and Y.J. Song. Penalty/finite element approximations of a class of unilateral problems in linear elasticity. *Quart. Appl. Math.*, 39:1–22, 1981.

[9] N. Kikuchi. A smoothing technique for reduced integration penalty methods in contact problems. *Int. J. Num. Meth. Engrg.*, 18:343–350, 1982.

[10] R.L. Taylor and P. Papadopoulos. A patch test for contact problems in two dimensions. In P. Wriggers and W. Wagner, editors, *Nonlinear Computational Mechanics*, pages 690–702. Springer, Berlin, 1991.

[11] P. Papadopoulos, R.E. Jones, and J.M. Solberg. A novel finite element formulation for frictionless contact problems. *Int. J. Num. Meth. Engrg.*, 38:2603–2617, 1995.

[12] P. Papadopoulos and J.M. Solberg. A Lagrange multiplier method for the finite element solution of frictionless contact problems. *Math. Comp. Model.*, 28:373–384, 1998.

[13] C. Truesdell and R. A. Toupin. Principles of classical mechanics and field theory. In S. Flügge, editor, *Handbuch der Physik*, volume III/1. Springer-Verlag, Berlin, 1960.

[14] W. Kosiński. *Field Singularities and Wave Analysis in Continuum Mechanics.* John Wiley and Sons, New York, 1986.

[15] J.-L. Lions and E. Magenes. *Non-homogeneous Boundary Value Problems and Applications*, volume I. Springer-Verlag, Berlin, 1972. trans. by P. Kenneth.

[16] H. Sagan. *Space Filling Curves.* Springer-Verlag, Berlin, 1994.

[17] R.L. Taylor. FEAP - A Finite Element Analysis Program, users manual. Univ. of California, Berkeley, 1998. http://www.ce.berkeley.edu/rlt.

[18] P. Papadopoulos and R.L. Taylor. A simple algorithm for three-dimensional finite element analysis of contact problems. *Comp. Struct.*, 46:1107–1118, 1993.

[19] J.C. Simo and F. Armero. Geometrically non-linear enhanced strain mixed methods and the method of incompatible modes. *Comp. Meth. Appl. Mech. Engrg.*, 33:1413–1439, 1992.

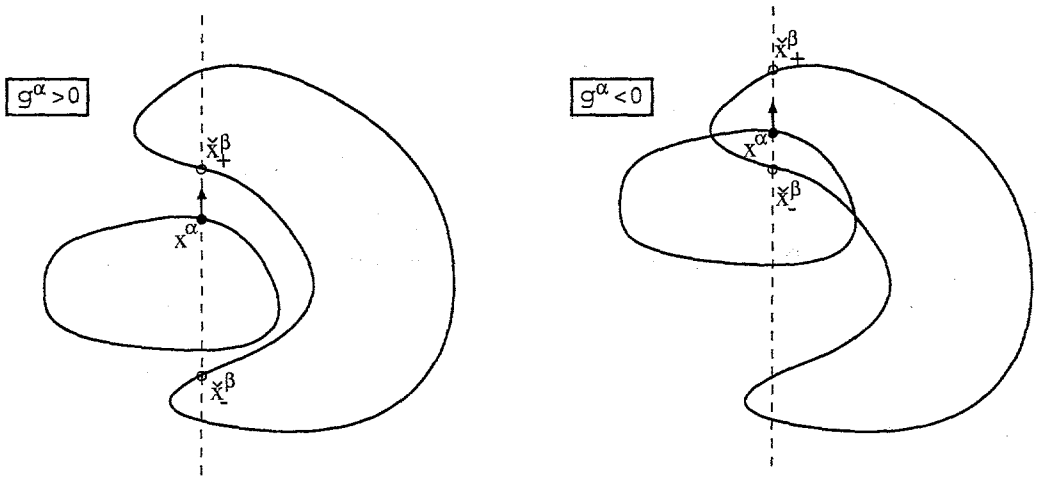

Figure 1: Definition of a distance function

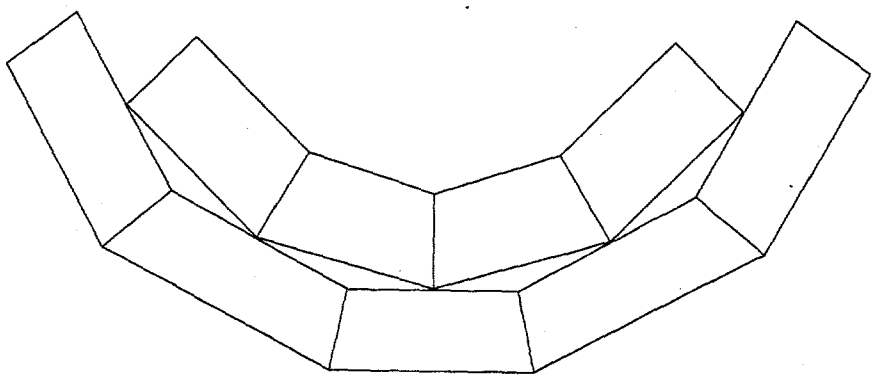

Figure 2: Non-conforming meshes

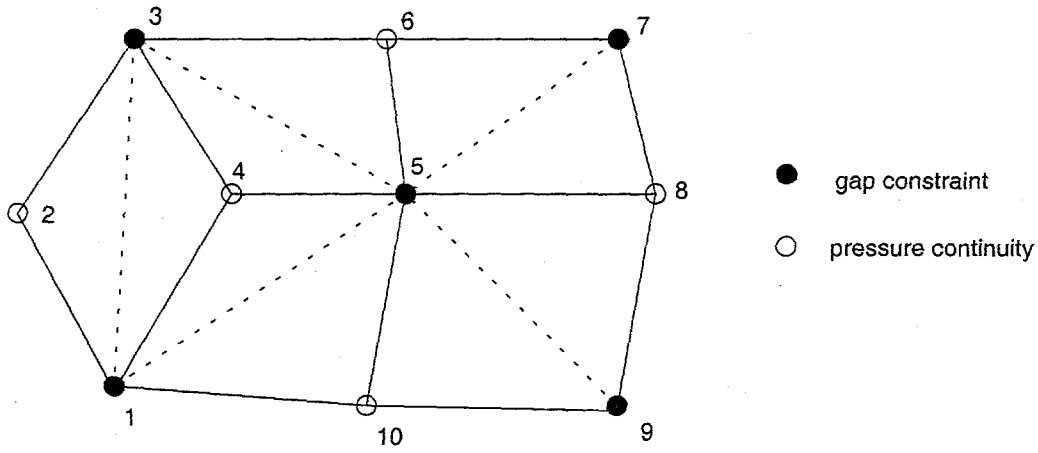

Figure 3: Patterning for a patch of elements

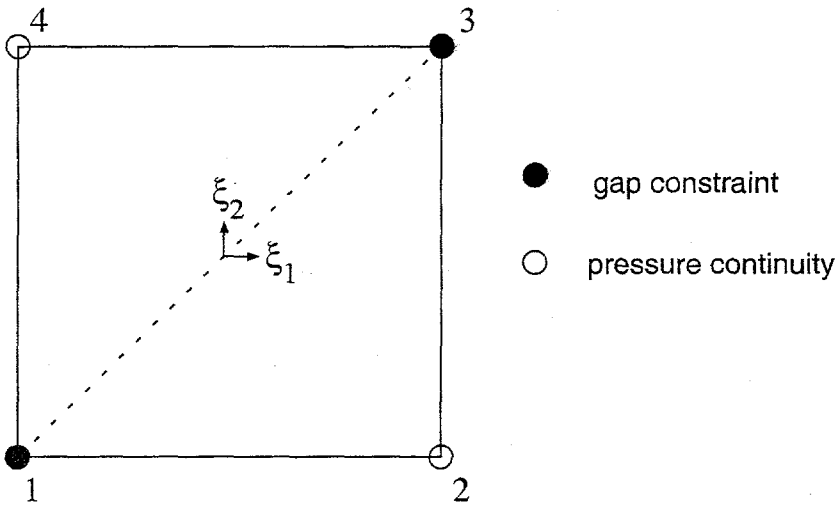

Figure 4: Reference contact element

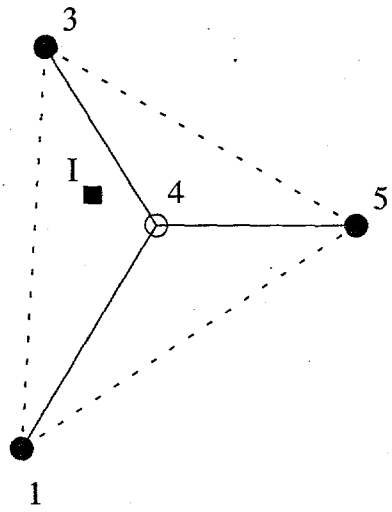

Figure 5: Point-collocation of pressure

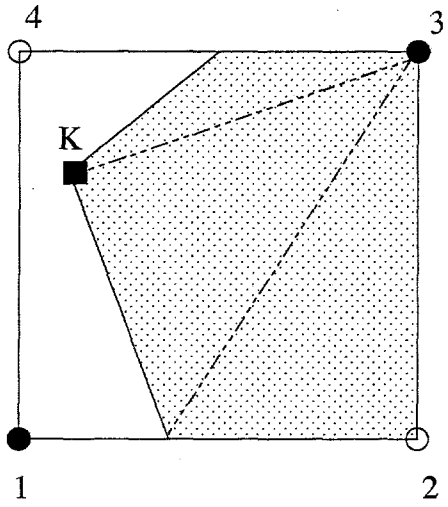

Figure 6: Contact element for partial contact

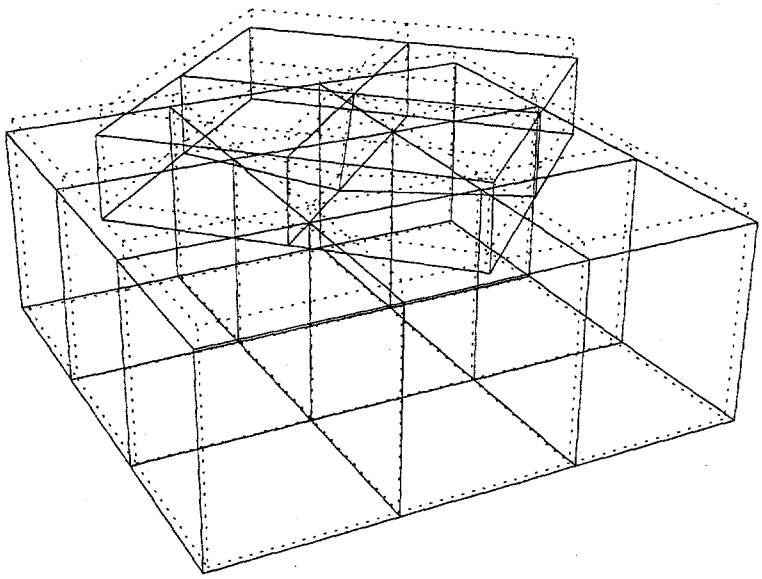

Figure 7: Patch test

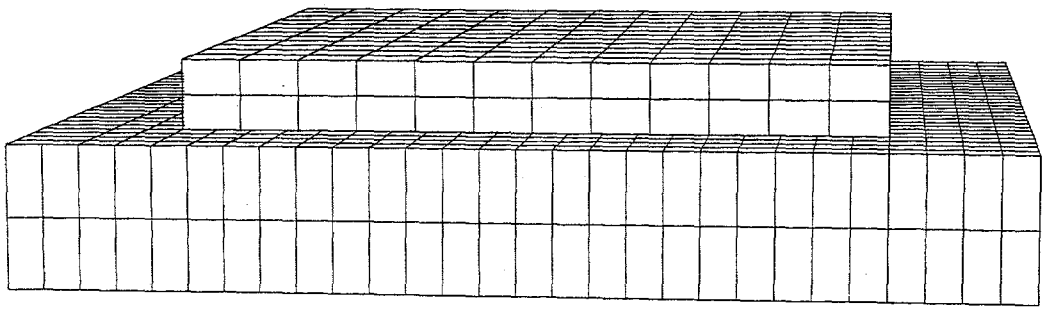

Figure 8: Mesh for punch and foundation

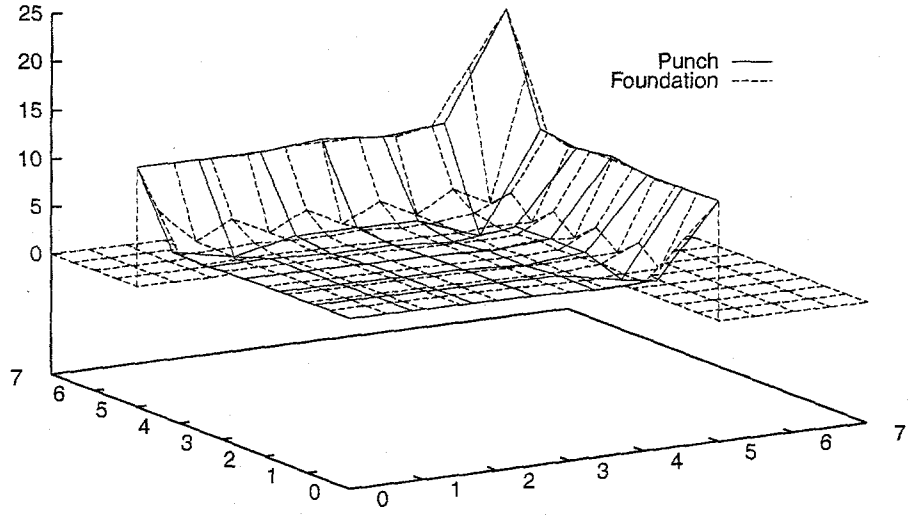

Figure 9: Pressure fields for punch problem

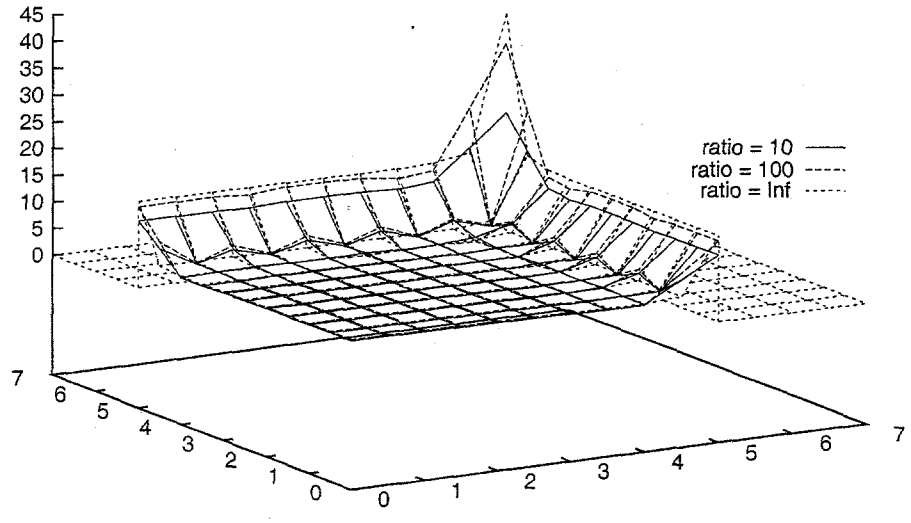

Figure 10: Comparison of pressure fields for punch problem

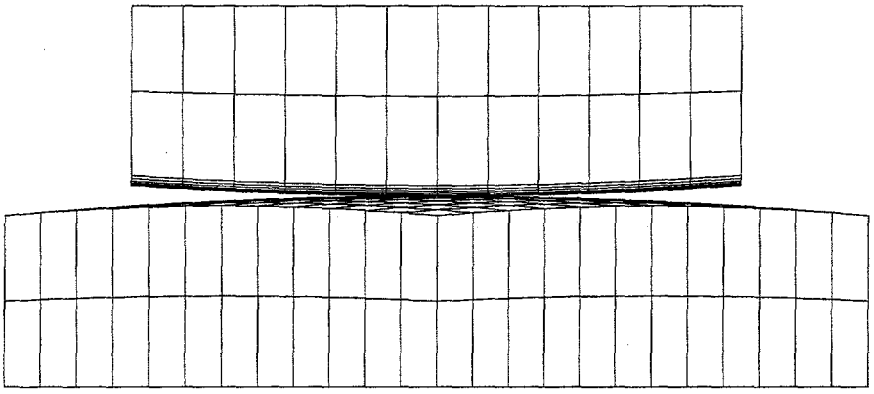

Figure 11: Undeformed mesh for analytical comparison

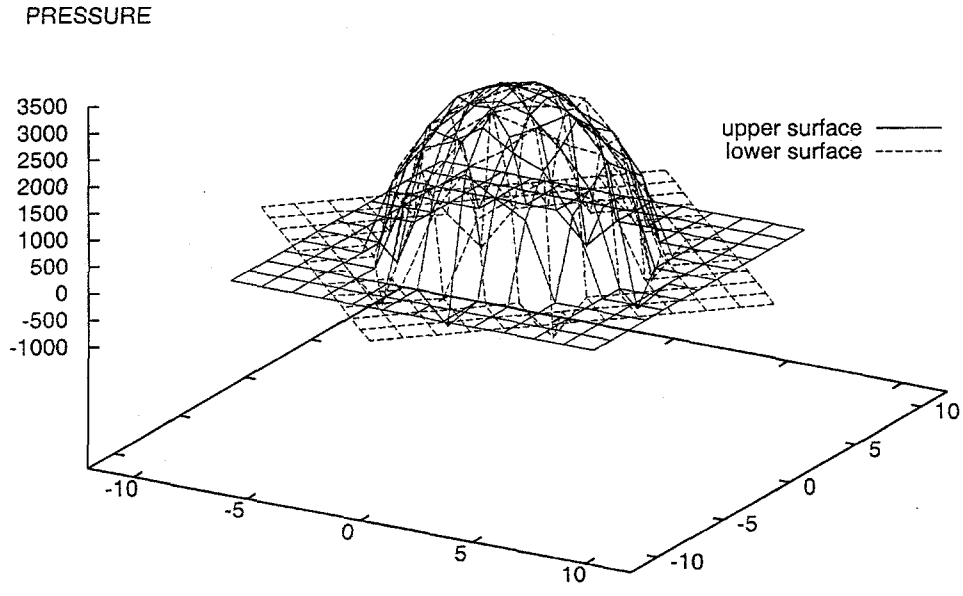

Figure 12: Pressure fields for Hertzian problem

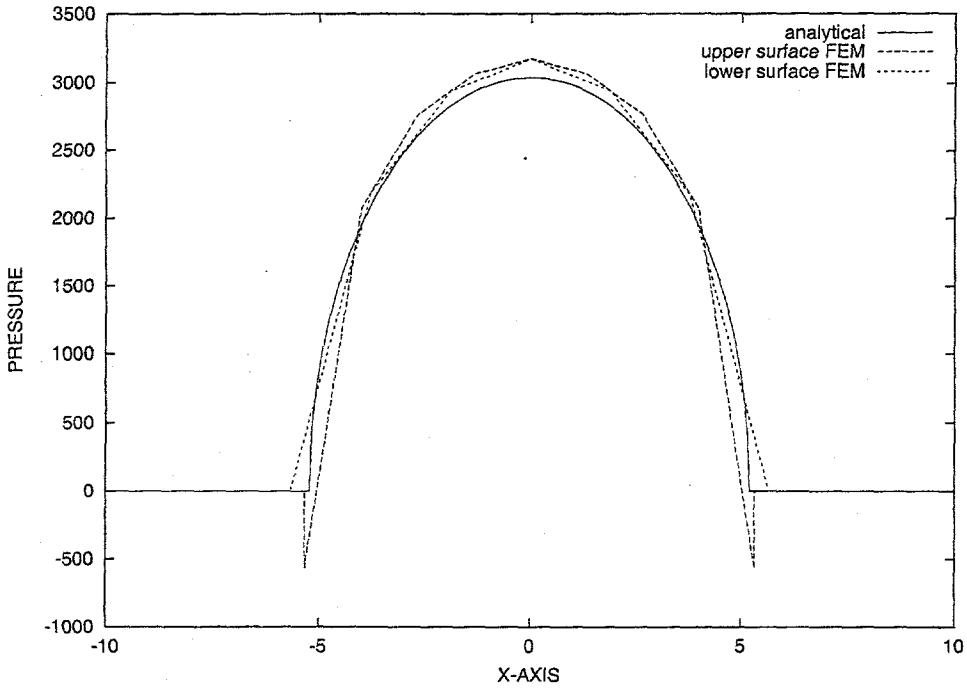

Figure 13: Comparison with analytical solution for Hertzian problem

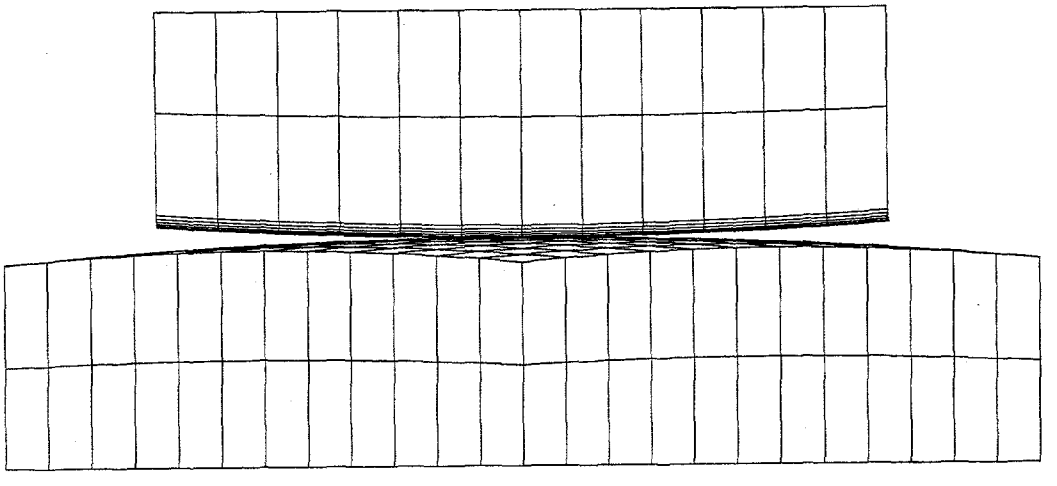

Figure 14: Undeformed mesh for one-pass comparison

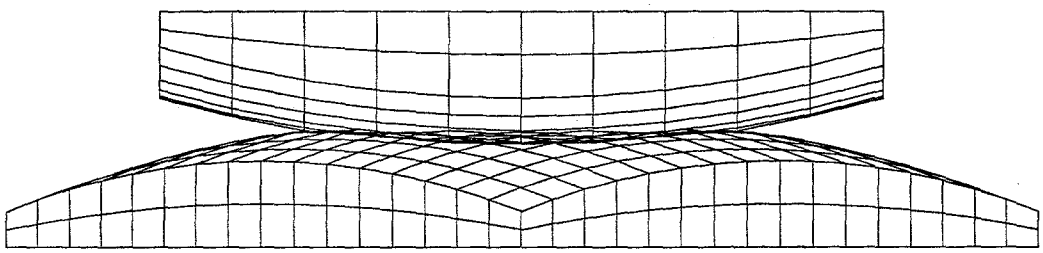

Figure 15: Deformed mesh using reduced constraint method

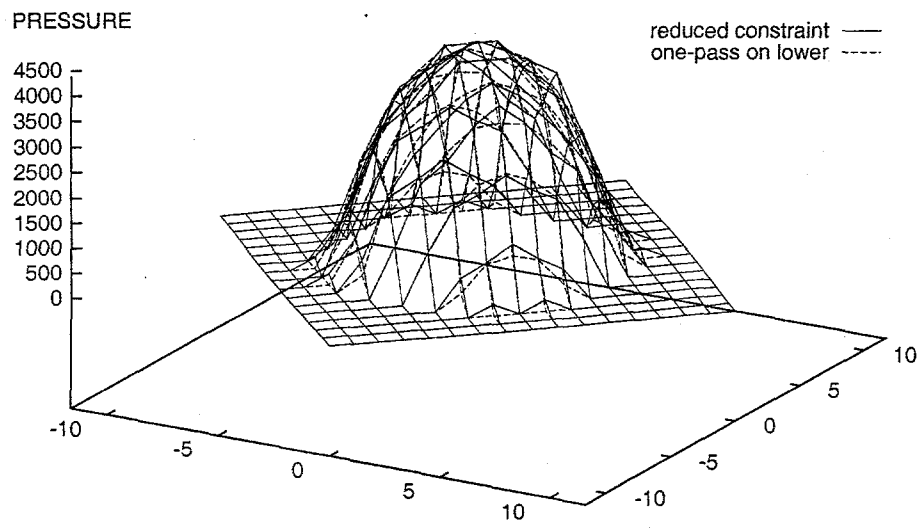

Figure 16: Comparison of reduced constraint formulation and one pass

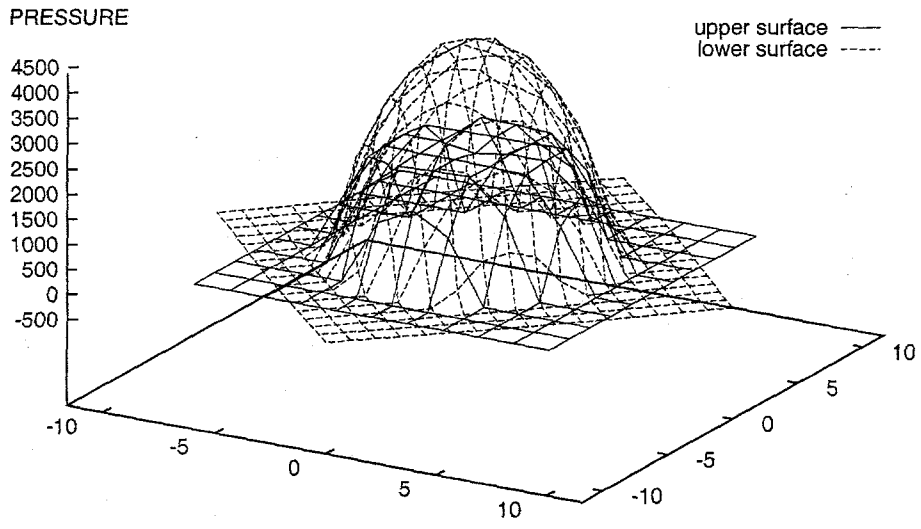

Figure 17: Comparison of two choices for the one-pass method

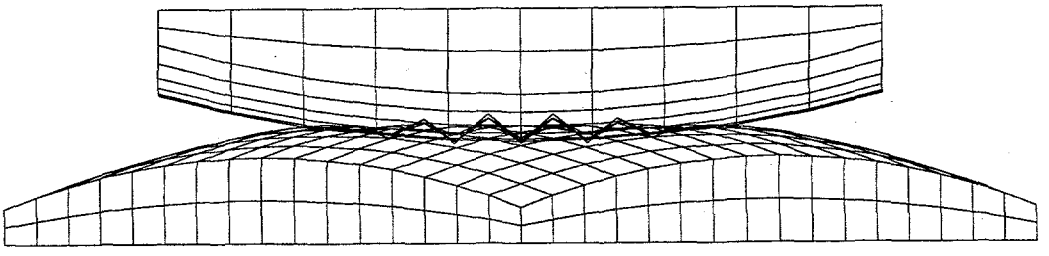

Figure 18: Deformed mesh for one-pass method using upper surface

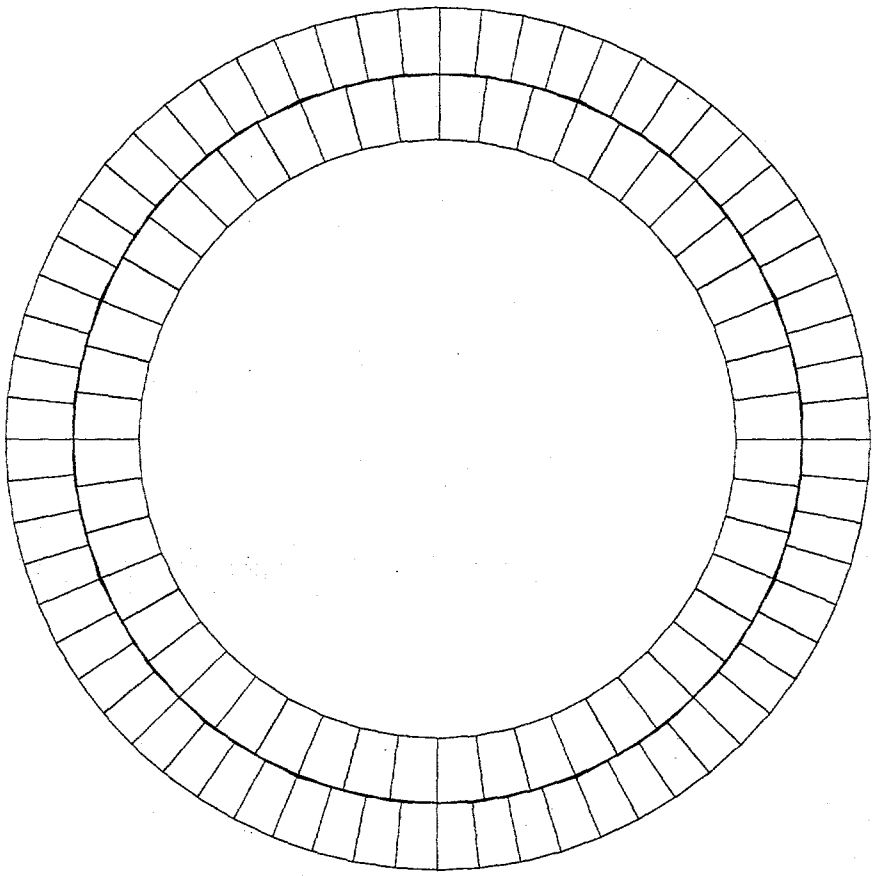

Figure 19: Deformed mesh using reduced constraint method

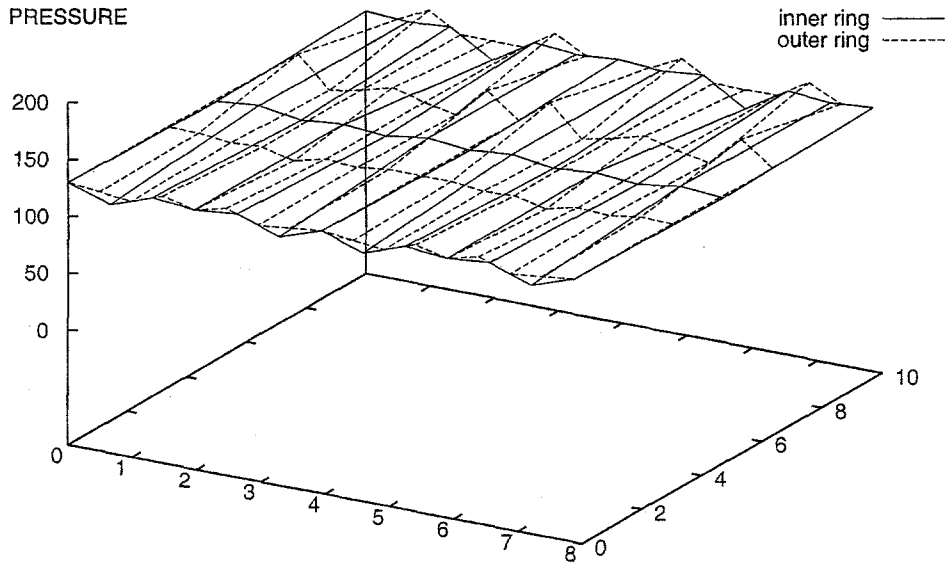

Figure 20: Pressure for reduced constraint method

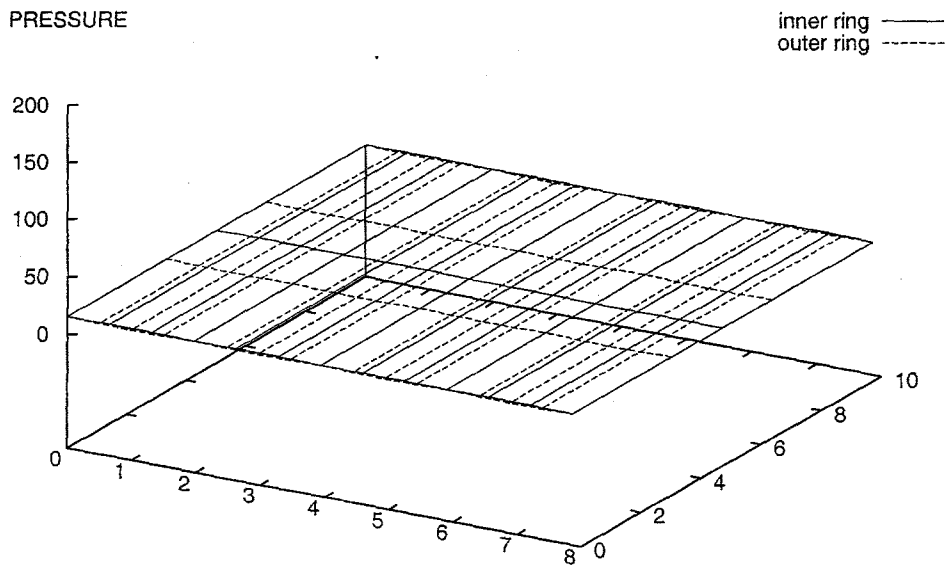

Figure 21: Pressure for two-pass penalty formulation, $\epsilon = 1.0 \times 10^2$

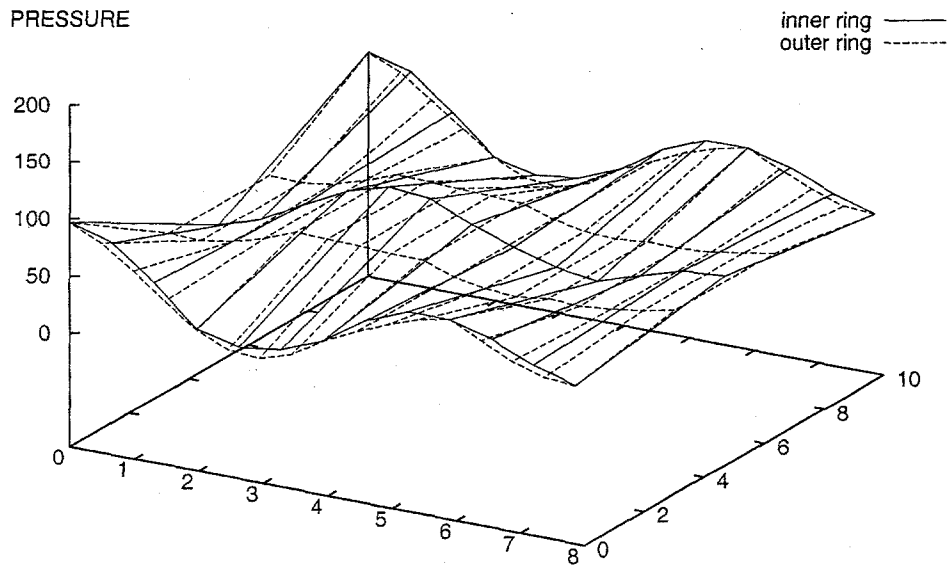

Figure 22: Pressure for two-pass penalty formulation, $\epsilon = 5.0 \times 10^2$

DISTRIBUTION:

1	MS 0819	K. H. Brown, 9231
1	MS 0826	W. L. Hermina, 9113
1	MS 0835	K. E. Casteel, 9121
1		J. S. Peery, 9121
1		K. H. Pierson, 9121
1	MS 0836	J. H. Biffle, 9121
1	MS 0841	T. C. Bickel, 9100
1	MS 0847	S. W. Attaway, 9121
1		M. K. Bhardwaj, 9121
1		M. L. Blanford, 9121
1		B. J. Driessen, 9121
1		A. S. Gullerud, 9121
1		M. W. Heinstein, 9121
1		S. W. Key, 9121
1		J. R. Koteras, 9121
1		J. A. Mitchell, 9121
1		V. L. Porter, 9121
1		T. J. Preston, 9121
1		G. M. Reese, 9121
1		C. M. Stone, 9121
1		J. W. Swegle, 9121
1	MS 0847	J. B. Aidun, 9123
1		J. M. Caruthers, 9123
1		R. S. Chambers, 9123
1		A. F. Fossum, 9123
1		D. C. Hamerand, 9123
1		S. C. Hwang, 9123
1		C. S. Lo, 9123
1		H. S. Morgan, 9123
1		M. K. Neilsen, 9123
1		E. D. Reedy, 9123
1		W. M. Scherzinger, 9123
1		W. Wellman, 9123

1	MS 9001	M. E. John, 8000
		Attn: R. C. Wayne, 2200, MS 9005
		J. Vitko, 8100, MS 9004
		W. J. McLean, 8300, MS 9054
		D. R. Henson, 8400, MS 9007
		P. N. Smith, 8500, MS 9002
		K. E. Washington, 8900, MS 9003
1	MS 9042	M. L. Chiesa, 8727
1		J. A. Crowell, 8727
1		J. J. Dike, 8727
1		J. L. Handrock, 8727
1		Y. R. Kan, 8727
1		B. L. Kistler, 8727
1		J. P. Lauffer, 8727
1		Y. Ohashi, 8727
1		R. Ortega, 8727
1		V. D. Revelli, 8727
1		R. A. Radovitzky, 8727
1		J. E. Robles, 8727
1		A. M. Sieber, 8727
1		L. E. Voelker, 8727
1		S. Wu, 8727
1	MS 9161	E. P. Chen, 8726
1		P. A. Klein, 8726
1		J. A. Zimmerman, 8726
1	MS 9221	C. M. Hartwig, 8510
1	MS 9405	T. M. Dyer, 8000
		Attn: R. Q. Hwang, 8721, MS 9161
		K. L. Wilson, 8722, MS 9402
		J. C. F. Wang, 8723, MS 9403
		G. J. Thomas, 8724, MS 9402
		W. A. Kawahara, 8725, MS 9042
		J. L. Handrock, 8727, MS 9042
		M. W. Perra, 8728, MS 9042
1		D. J. Bammann, 8726
1		J. W. Foulk, 8726
1		Y. Hammi, 8726
1		M. F. Horstemeyer, 8726
1		D. A. Hughes, 8726
1		R. E. Jones, 8726
1		M. T. Lyttle, 8726

1		E. B. Marin, 8726
1		R. A. Regueiro, 8726
3	MS 9018	Central Technical Files, 8940-2
1	MS 0899	Technical Library, 4916
1	MS 9021	Technical Communications Dept., 8815
1	MS 9021	Technical Communications Dept., 8815 for DOE/OSTI